

1 Dual Neural Network (DuNN) Method
2 for Elliptic Partial Differential Equations and Systems

3 Min Liu¹, Zhiqiang Cai², Karthik Ramani¹

4 **Abstract**

5 This paper presents the Dual Neural Network (DuNN) method, a physics-driven numerical method designed
6 to solve elliptic partial differential equations and systems using deep neural network functions and a dual
7 formulation. The underlying elliptic problem is formulated as an optimization of the complementary energy
8 functional in terms of the dual variable, where the Dirichlet boundary condition is weakly enforced in
9 the formulation. To accurately evaluate the complementary energy functional, we employ a novel discrete
10 divergence operator. This discrete operator preserves the underlying physics and naturally enforces the
11 Neumann boundary condition without penalization. For problems without reaction term, we propose an
12 outer-inner iterative procedure that gradually enforces the equilibrium equation through a pseudo-time
13 approach.

14 *Keywords:* Elliptic PDE, Linear Elasticity, Deep Neural Network, Dual formulation.

15 **1. Introduction**

16 Neural networks (NNs) have demonstrated remarkable performance in computer vision, natural language
17 processing, and various other artificial intelligence tasks. Recently, their application to solving partial
18 differential equations (PDEs) has gained significant traction [1, 2, 3, 4, 5, 6, 7, 8]. As a new class of
19 approximating functions, NNs exhibit exceptional approximation capabilities, surpassing those of continuous
20 and discontinuous piecewise polynomials on *fixed* meshes (see, e.g., [9, 10, 11]). In particular, a NN function
21 can automatically adapt to a target function through a “moving mesh” behavior, making it one of the most
22 promising candidates among all known functional classes for addressing various challenging problems in
23 scientific computing.

24 Since NN functions are nonlinear with respect to their parameters, the discretization of a PDE using
25 NN can be formulated as an optimization problem through either natural minimization or manufactured
26 least-squares (LS) principles. Consequently, existing NN-based numerical methods for solving PDEs fall

Email addresses: liu66@purdue.edu (Min Liu), caiz@purdue.edu (Zhiqiang Cai), ramani@purdue.edu (Karthik Ramani)

¹School of Mechanical Engineering, Purdue University, 585 Purdue Mall, West Lafayette, IN 47907-2088

²Department of Mathematics, Purdue University, 150 N. University Street, West Lafayette, IN 47907-2067

27 into two main categories: (1) energy-based methods [1, 12, 13, 8], which utilize the principle of natural
 28 energy minimization, and (2) deep LS methods employing various types of manufactured least squares
 29 [2, 5, 3, 7, 14]. Most elliptic problems adhere to the basic minimization principle in the form of an energy
 30 functional. Therefore, when using NN as approximating functions, it is natural to discretize the underlying
 31 problem based on the energy formulation.

32 For applications in continuum mechanics, the dual variable, such as stress in elasticity or flux in porous
 33 media flow, often stands as the primary physical quantity of interest. While it can be derived from methods
 34 based on the primal variable, such as displacement or pressure, through differentiation, this approach comes
 35 at the cost of degrading the order of the approximation for the dual variables. In this paper, we propose dual
 36 neural network (DuNN), a numerical method that solves elliptic partial differential equations and systems
 37 using NNs as the approximating functions for the dual variable, and the complementary energy functional
 38 as the loss function. Compared to existing physics-driven NN-based approaches, DuNN offers the following
 39 advantages:

- 40 (1) In many continuum mechanics problems, accurately computing stress/flux is often more important
 41 than displacement/pressure. DuNN achieves this directly without differentiation, as stress/flux is the
 42 sole independent variable in the complementary energy functional.
- 43 (2) DuNN is applicable to a wider range of problems, including those with or without discontinuities or
 44 singularities. Additionally, DuNN is suitable for incompressible materials, which are not adequately
 45 addressed by standard energy-based methods.
- 46 (3) DuNN enforces both Dirichlet and Neumann boundary conditions naturally, eliminating the need for
 47 any penalty term in the loss functional. This results in fewer hyperparameters to adjust.

48 The remainder of the paper is structured as follows. Section 2 reformulates an elliptic PDE into a
 49 minimization problem using a dual formulation. Section 3 presents the DuNN method in detail, and we
 50 show our numerical studies in Section 4 and conclude the paper in Section 5.

51 **2. Dual Formulation of Elliptic Partial Differential Equations**

52 Let Ω be a bounded, open, connected subset of \mathbb{R}^d ($d = 2$ or 3) with a Lipschitz continuous boundary
 53 $\partial\Omega$. Let $\mathbf{n} = (n_1, \dots, n_d)$ be the outward unit vector normal to the boundary. Partition the boundary $\partial\Omega$ of
 54 the domain Ω into two open subsets Γ_D and Γ_N such that $\partial\Omega = \Gamma_D \cup \Gamma_N$ and $\Gamma_D \cap \Gamma_N = \emptyset$. For simplicity,
 55 we assume that Γ_D is not empty (i.e., $\text{mes}(\Gamma_D) \neq 0$). Otherwise, solutions of partial differential equations
 56 considered in this paper are unique up to an additive constant or rigid motions.

57 We will use the standard notation and definitions for the Sobolev space $\mathbf{H}^s(\Omega)^d$ and $\mathbf{H}^s(\Gamma)$ for a subset
 58 Γ of the boundary of the domain $\Omega \in \mathbb{R}^d$. The standard associated inner product and norms are denoted by

59 $(\cdot, \cdot)_{s, \Omega, d}$ and $(\cdot, \cdot)_{s, \Gamma, d}$ and by $\|\cdot\|_{s, \Omega, d}$ and $\|\cdot\|_{s, \Gamma, d}$, respectively. When there is no ambiguity, the subscript
60 Ω and d in the designation of norms will be suppressed. When $s = 0$, $\mathbf{H}^0(\Omega)^d$ coincides with $\mathbf{L}^2(\Omega)^d$. In
61 this case, the inner product and norm will be denoted by (\cdot, \cdot) and $\|\cdot\|$, respectively.

62 2.1. Second-order Elliptic Problems

Consider the following self-adjoint second-order scalar elliptic partial differential equation:

$$\begin{cases} -\operatorname{div}(A\nabla u) + cu = f, & \text{in } \Omega, \\ u = g_D, & \text{on } \Gamma_D, \\ \mathbf{n} \cdot A\nabla u = g_N, & \text{on } \Gamma_N, \end{cases} \quad (1)$$

63 where div is the divergence operator; $f \in L^2(\Omega)$, $c \in L^\infty(\Omega)$, $g_D \in H^{1/2}(\Gamma_D)$, $g_N \in H^{-1/2}(\Gamma_N)$; $A(\mathbf{x})$ is
64 a $d \times d$ symmetric matrix-valued function in $L^2(\Omega)^{d \times d}$; and \mathbf{n} is the outward unit vector normal to the
65 boundary. We assume that A is uniformly positive definite and that $c(\mathbf{x}) \geq 0$ for almost all $\mathbf{x} \in \Omega$.

Introducing the dual (flux) variable $\boldsymbol{\sigma} = -A\nabla u$, then the dual problem is to maximize the complementary energy functional (see, e.g., [15, 16]). Specifically, denote the collection of square-integrable vector fields whose divergence are also square-integrable by

$$H(\operatorname{div}; \Omega) = \{\boldsymbol{\tau} \in L^2(\Omega)^d : \operatorname{div} \boldsymbol{\tau} \in L^2(\Omega)\},$$

which is a Hilbert space equipped with norm

$$\|\boldsymbol{\tau}\|_{\operatorname{div}, \Omega} = (\|\boldsymbol{\tau}\|_{0, \Omega}^2 + \|\operatorname{div} \boldsymbol{\tau}\|_{0, \Omega}^2)^{1/2}.$$

Denote the subset of $H(\operatorname{div}; \Omega)$ satisfying the Neumann boundary condition by

$$H_{g, N}(\operatorname{div}; \Omega) = H(\operatorname{div}; \Omega) \cap \{\mathbf{n} \cdot \boldsymbol{\sigma}|_{\Gamma_N} = g_N\}$$

66 and the negative complementary functional by

$$J_1(\boldsymbol{\tau}; \gamma) = \frac{1}{2} \left\{ \|A^{-1/2} \boldsymbol{\tau}\|_{0, \Omega}^2 + \|\gamma^{1/2} (\operatorname{div} \boldsymbol{\tau} - f)\|_{0, \Omega}^2 \right\} + (g_D, \boldsymbol{\tau} \cdot \mathbf{n})_{0, \Gamma_D}, \quad (2)$$

where γ is given by

$$\gamma = \begin{cases} c^{-1}(\mathbf{x}), & \text{if } c > 0, \\ 0, & \text{if } c = 0. \end{cases} \quad (3)$$

Then the dual problem is to find $\boldsymbol{\sigma} \in \boldsymbol{\Sigma}_g$ such that

$$J_1(\boldsymbol{\sigma}; \gamma) = \min_{\boldsymbol{\tau} \in \boldsymbol{\Sigma}_g} J_1(\boldsymbol{\tau}; \gamma), \quad (4)$$

where $\boldsymbol{\Sigma}_g$ is given by

$$\boldsymbol{\Sigma}_g = \begin{cases} H_{g, N}(\operatorname{div}; \Omega), & \text{if } c > 0, \\ \{\boldsymbol{\tau} \in H_{g, N}(\operatorname{div}; \Omega) : \operatorname{div} \boldsymbol{\tau} = f\}, & \text{if } c = 0. \end{cases} \quad (5)$$

67 The following proposition is well-known (see, e.g., [17]).

Proposition 1. *Problem (4) has a unique solution $\boldsymbol{\sigma} \in \boldsymbol{\Sigma}_g$. Moreover, the solution $\boldsymbol{\sigma}$ satisfies the following a priori estimate:*

$$\|\boldsymbol{\sigma}\|_{div,\Omega} \leq C \left(\|f\|_{0,\Omega} + \|g_D\|_{1/2,\Gamma_D} + \|g_N\|_{-1/2,\Gamma_N} \right).$$

68 2.2. Linear Elasticity and Stokes Equations

69 In linear elasticity problems, it is often more useful to compute accurately stress rather than displacement.
70 This can be achieved by using the dual formulation that maximizes the complementary energy functional
71 for the stress (dual) variable $\boldsymbol{\sigma}$. This section describes the dual formulation for both linear elasticity and
72 Stokes equations.

To this end, denote by \mathbf{u} and $\boldsymbol{\sigma}$ the displacement/velocity field and the stress tensor, respectively. Then the stress-displacement/velocity formulation (see, e.g., [17, 18, 19]) has the form

$$\begin{cases} -\mathbf{div} \boldsymbol{\sigma} + c \mathbf{u} = \mathbf{f}, & \text{in } \Omega, \\ \mathcal{A}_\lambda \boldsymbol{\sigma} - \boldsymbol{\epsilon}(\mathbf{u}) = \mathbf{0}, & \text{in } \Omega \end{cases} \quad (6)$$

with boundary conditions

$$\mathbf{u}|_{\Gamma_D} = \mathbf{g}_D \quad \text{and} \quad (\boldsymbol{\sigma} \mathbf{n})|_{\Gamma_N} = \mathbf{g}_N,$$

73 where \mathbf{div} is the divergence operator; $c \in L^\infty(\Omega)$ is a given scalar-valued function; $\mathbf{f} \in \mathbf{L}^2(\Omega)^d$, $\mathbf{g}_D \in$
74 $\mathbf{H}^{1/2}(\Gamma_D)^d$, and $\mathbf{g}_N \in \mathbf{H}^{-1/2}(\Gamma_N)^d$ are given vector-valued functions defined on Ω , Γ_D , and Γ_N , rep-
75 resenting body force, boundary displacement/velocity, and boundary traction force, respectively; $\boldsymbol{\epsilon}(\mathbf{u}) =$
76 $\frac{1}{2} (\nabla \mathbf{u} + (\nabla \mathbf{u})^T)$ is the strain tensor; and \mathcal{A}_λ is the compliance tensor of fourth order

$$\mathcal{A}_\lambda \boldsymbol{\tau} = \frac{1}{2\mu} \left(\boldsymbol{\tau} - \frac{\lambda}{2\mu + d\lambda} (\text{tr} \boldsymbol{\tau}) \boldsymbol{\delta}_{d \times d} \right) \quad \text{with} \quad \text{tr} \boldsymbol{\tau} = \sum_{i=1}^d \tau_{ii}.$$

Here, $\boldsymbol{\delta}_{d \times d}$ is the d -dimensional identity tensor; μ and λ are the material Lamé constants. The material is said to be nearly incompressible if $\lambda \gg 1$ or incompressible if $\lambda = \infty$. It is easy to see that

$$\mathcal{A}_\infty \boldsymbol{\tau} = \frac{1}{2\mu} \left(\boldsymbol{\tau} - \frac{1}{d} (\text{tr} \boldsymbol{\tau}) \boldsymbol{\delta}_{d \times d} \right).$$

77 Hence the formulation in (6) is valid for both compressible and incompressible materials.

Denote the collection of all symmetric stress whose divergence is square integrable by

$$\mathbf{H}^s(\text{div}; \Omega) = \{ \boldsymbol{\tau} \in \mathbf{L}^2(\Omega)^{d \times d} : \boldsymbol{\tau}^t = \boldsymbol{\tau}, \mathbf{div} \boldsymbol{\tau} \in \mathbf{L}^2(\Omega)^d \}$$

and its subset satisfying the Neumann boundary condition by

$$\mathbf{H}_{g,N}^s(\text{div}; \Omega) = \left\{ \boldsymbol{\tau} \in \mathbf{H}^s(\text{div}; \Omega) : \boldsymbol{\tau} \mathbf{n}|_{\Gamma_N} = \mathbf{g}_N \right\}.$$

The negative complementary energy functional is given by

$$J_2(\boldsymbol{\tau}; \gamma) = \frac{1}{2} \left\{ (\mathcal{A}_\lambda \boldsymbol{\tau}, \boldsymbol{\tau})_{0,\Omega} + \|\gamma(\mathbf{div} \boldsymbol{\tau} - \mathbf{f})\|_{0,\Omega}^2 \right\} - \int_{\Gamma_D} \mathbf{g}_D \cdot (\boldsymbol{\tau} \mathbf{n}) ds, \quad (7)$$

where the γ is given in (3) and

$$(\mathcal{A}_\lambda \boldsymbol{\tau}, \boldsymbol{\tau})_{0,\Omega} = \frac{1}{2\mu} \int_\Omega |\mathcal{A}_\infty \boldsymbol{\tau}|^2 dx + \frac{1}{d(2\mu + d\lambda)} \int_\Omega |\text{tr} \boldsymbol{\tau}|^2 dx.$$

Then the dual formulation of problem (6) is to seek $\boldsymbol{\sigma} \in \boldsymbol{\Sigma}_g$ such that

$$J_2(\boldsymbol{\sigma}; \gamma) = \min_{\boldsymbol{\tau} \in \boldsymbol{\Sigma}_g} J_2(\boldsymbol{\tau}; \gamma), \quad (8)$$

where $\boldsymbol{\Sigma}_g$ is given by

$$\boldsymbol{\Sigma}_g = \begin{cases} \mathbf{H}_{g,N}^s(\text{div}; \Omega), & \text{if } c > 0, \\ \{\boldsymbol{\tau} \in \mathbf{H}_{g,N}^s(\text{div}; \Omega) : \mathbf{div} \boldsymbol{\tau} + \mathbf{f} = \mathbf{0}\}, & \text{if } c = 0. \end{cases} \quad (9)$$

78 The following existence, uniqueness, and stability are also well-known [17].

Proposition 2. *Problem (8) has a unique solution $\boldsymbol{\sigma} \in \boldsymbol{\Sigma}_g$. Moreover, there exists a positive constant such that*

$$\|\boldsymbol{\sigma}\|_{\text{div},\Omega} \leq C \left(\|\mathbf{f}\|_{0,\Omega} + \|\mathbf{g}_D\|_{1/2,\Gamma_D} + \|\mathbf{g}_N\|_{-1/2,\Gamma_N} \right).$$

79 *2.3. Abstract Setting*

For convenience, this section uses an abstract setting to unify the dual formulations in (4) and (8). To this end, for any $\boldsymbol{\sigma}, \boldsymbol{\tau} \in \boldsymbol{\Sigma}_g$, introduce the following bilinear and linear forms

$$a(\boldsymbol{\sigma}, \boldsymbol{\tau}; \gamma) = \begin{cases} (A^{-1} \boldsymbol{\sigma}, \boldsymbol{\tau})_{0,\Omega} + (\gamma \text{div} \boldsymbol{\sigma}, \text{div} \boldsymbol{\tau})_{0,\Omega}, & \text{problem (1),} \\ (\mathcal{A}_\lambda \boldsymbol{\sigma}, \boldsymbol{\tau})_{0,\Omega} + (\gamma \mathbf{div} \boldsymbol{\sigma}, \mathbf{div} \boldsymbol{\tau})_{0,\Omega}, & \text{problem (6)} \end{cases}$$

and

$$b(\boldsymbol{\tau}; f, \gamma) = \begin{cases} (\gamma f, \text{div} \boldsymbol{\tau})_{0,\Omega} - \int_{\Gamma_D} \mathbf{g}_D \boldsymbol{\tau} \cdot \mathbf{n} ds, & \text{problem (1),} \\ (\gamma \mathbf{f}, \mathbf{div} \boldsymbol{\tau})_{0,\Omega} + \int_{\Gamma_D} \mathbf{g}_D \cdot (\boldsymbol{\tau} \mathbf{n}) ds, & \text{problem (6)} \end{cases}$$

respectively, where $\boldsymbol{\Sigma}_g$ is a subset of $H(\text{div}; \Omega)^d$ satisfying constraints like essential boundary condition, symmetry, and/or the equilibrium equation (see (5) and (9)). Define the negative complementary functional by

$$J(\boldsymbol{\tau}; \gamma) = \frac{1}{2} a(\boldsymbol{\tau}, \boldsymbol{\tau}; \gamma) - b(\boldsymbol{\tau}; f, \gamma) + \frac{1}{2} c^2(f; \gamma), \quad (10)$$

where $c(f; \gamma) = \|\gamma^{1/2} f\|_{0,\Omega}$ or $c(f; \gamma) = \|\gamma^{1/2} \mathbf{f}\|_{0,\Omega}$ for problems (1) or (6), respectively, is a constant. Then the dual formulation is to seek $\boldsymbol{\sigma} \in \boldsymbol{\Sigma}_g$ such that

$$J(\boldsymbol{\sigma}; \gamma) = \min_{\boldsymbol{\tau} \in \boldsymbol{\Sigma}_g} J(\boldsymbol{\tau}; \gamma). \quad (11)$$

Assume that there exists a positive $\gamma_0 > 0$ such that $\gamma(\mathbf{x}) \geq \gamma_0$. Then the solution $\boldsymbol{\sigma} \in \boldsymbol{\Sigma}_g$ of (11) satisfies

$$a(\boldsymbol{\sigma}, \boldsymbol{\tau}; \gamma) = b(\boldsymbol{\tau}; f, \gamma), \quad \forall \boldsymbol{\tau} \in \boldsymbol{\Sigma}_0. \quad (12)$$

80 3. Dual neural network (DuNN) method

81 In this section, we describe the dual neural network (DuNN) method. Simply, the DuNN method is a
 82 discretization method for solving a partial differential equation or system based on the dual formulation
 83 of the underlying problem. DuNN includes a standard fully connected DNN as the class of approximating
 84 functions and the negative complementary energy functional $J_{\mathcal{T}}(\boldsymbol{\sigma}; \gamma)$ as the loss functional estimated by
 85 numerical integration and differentiation (discrete divergence operator). The general structure of the DuNN
 86 is illustrated in Figure 1.

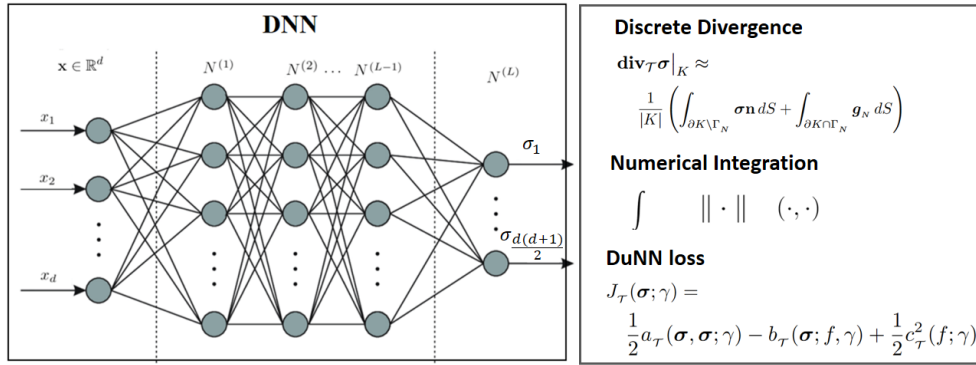


Figure 1: DuNN architecture. A fully connected L -layer network is employed to generate the map from an arbitrary spatial point \mathbf{x} in Ω to its flux $\boldsymbol{\sigma}(\mathbf{x})$, quadrature based numerical integration and discrete divergence operator are used to approximate the discrete complementary energy functional $J_{\mathcal{T}}(\boldsymbol{\sigma}; \gamma)$ as the DuNN loss.

87 3.1. Deep Neural Network

For $j = 1, \dots, l-1$, let $N^{(j)}: \mathbb{R}^{n_{j-1}} \rightarrow \mathbb{R}^{n_j}$ be the vector-valued ridge function of the form

$$N^{(j)}(\mathbf{x}^{(j-1)}) = \zeta(\boldsymbol{\omega}^{(j)} \mathbf{x}^{(j-1)} - \mathbf{b}^{(j)}) \quad \text{for } \mathbf{x}^{(j-1)} \in \mathbb{R}^{n_{j-1}}, \quad (13)$$

88 where $\boldsymbol{\omega}^{(j)} \in \mathbb{R}^{n_j \times n_{j-1}}$ and $\mathbf{b}^{(j)} \in \mathbb{R}^{n_j}$ are the respective weights and biases to be determined; $\mathbf{x}^{(0)} = \mathbf{x}$; and
 89 $\zeta(t)$ is the activation function and its application to a vector is defined component-wise. There are many
 90 choices of activation functions such as ReLU, logistic, Gaussian, hyperbolic tangent, and sigmoids (see, e.g.
 91 [20]).

92 Let $\boldsymbol{\omega}^{(l)} \in \mathbb{R}^{d_o \times n_{l-1}}$ and $\mathbf{b}^{(l)} \in \mathbb{R}^{d_o}$ be the output weights and bias, respectively, where $d_o = d$ for
 93 problem (1) and $d_o = 3(d-1)$ for problem (6). Then a l -layer neural network generates the following set of
 94 vector-valued functions in \mathbb{R}^{d_o}

$$\begin{aligned} \mathcal{M}_M &= \mathcal{M}_M(\zeta) = \mathcal{M}_M(\zeta, l) \\ &= \left\{ \boldsymbol{\omega}^l \left(N^{(l-1)} \circ \dots \circ N^{(1)}(\mathbf{x}) \right) - \mathbf{b}^l : \boldsymbol{\omega}^{(j)} \in \mathbb{R}^{n_j \times n_{j-1}}, \mathbf{b}^{(j)} \in \mathbb{R}^{n_j} \text{ for all } j \right\}, \end{aligned} \quad (14)$$

95 where the symbol \circ denotes the composition of functions.

96 This class of functions is rich enough to accurately approximate any continuous function defined on a
 97 compact set $\Omega \in \mathbb{R}^d$ (see [21, 22] for the universal approximation property). However, this is not the main
 98 reason why NNs are so effective in practice. One way to understand its approximation power is from the
 99 point view of polynomial spline functions with free knots ([23]). The set $\mathcal{M}_M(\zeta, 2)$ may be regarded as a
 100 beautiful extension of free knot splines from one dimensional scalar-valued function to multi-dimensional
 101 vector-valued function. It has been shown that the approximation of functions by splines can generally be
 102 dramatically improved if the knots are free.

103 3.2. DuNN method

104 The DuNN method is a discretization method for approximating the solution of partial differential equa-
 105 tions or systems based on the dual formulation and using neural networks as approximating functions. The
 106 resulting discrete, non-convex minimization problem of the DuNN method is sophisticated and computa-
 107 tionally intensive and can be numerically solved using existing iterative methods such as ADAM, BFGS,
 108 etc.

109 Notice that \mathcal{M}_M is a subset of $\mathcal{C}^0(\Omega)^{d_\sigma}$ due to the continuity of the activation function $\zeta(t)$. Hence,
 110 $\mathcal{M}_M(\zeta) \cap \Sigma_g$ is the set of admissible functions for the minimization problem in (11). The DuNN method
 111 is then to seek an approximation by minimizing the negative complimentary functional in the set of neural
 112 network functions $\mathcal{M}_M(\zeta) \cap \Sigma_g$. To design a viable DuNN method, we need to address the following
 113 three numerical issues: (1) numerical integration, (2) discrete divergence operator, and (3) the constraints
 114 (Neumann boundary conditions and symmetry of the stress for the PDE system) on Σ_g .

First, unlike finite element methods, numerical integration for NN-based methods is a nontrivial matter.
 The difficulty stems from the fact that the NN approximation function is unknown, and hence so is its
 physical partition [24, 14]. To overcome this obstacle, we recently introduced an adaptive quadrature
 method in [8] to achieve the prescribe accuracy with fewer integration points. In this paper, we consider
 only the composite midpoint quadrature rule on a fixed partition for simplicity of presentation and refer
 readers to [8] for accurate and efficient numerical integration. To this end, partition the domain Ω by a
 collection of subdomains

$$\mathcal{T} = \{K : K \text{ is an open subdomain of } \Omega\}$$

such that

$$\bar{\Omega} = \cup_{K \in \mathcal{T}} \bar{K} \quad \text{and} \quad K \cap T = \emptyset, \quad \forall K, T \in \mathcal{T}.$$

That is, the union of all subdomains of \mathcal{T} equals to the whole domain Ω , and any two distinct subdomains
 of \mathcal{T} have no intersection. The resulting partitions of the boundary Γ_D and Γ_N are

$$\mathcal{E}_D = \{E = \partial K \cap \Gamma_D : K \in \mathcal{T}\} \quad \text{and} \quad \mathcal{E}_N = \{E = \partial K \cap \Gamma_N : K \in \mathcal{T}\},$$

respectively. Denote by \mathbf{x}_K and $|K|$ the respective centroid and volume of element $K \in \mathcal{T}$, and by \mathbf{x}_E and $|E|$ the respective centroid and area of boundary element $E \in \mathcal{E}_S$ for $S = D$ and N . Then

$$\int_{\Omega} v(\mathbf{x}) d\mathbf{x} \approx \sum_{K \in \mathcal{T}} v(\mathbf{x}_K) |K| \quad \text{and} \quad \int_{\Gamma_S} v(\mathbf{x}) ds \approx \sum_{E \in \mathcal{E}_S} v(\mathbf{x}_E) |E|. \quad (15)$$

115 Second, numerical differentiation becomes a critical component for a viable DuNN method. This difficulty
 116 stems from the fact that the admissible solution set Σ_g whose functions may not be continuous in tangential
 117 directions across some interfaces. Hence, the divergence differential operator can not be approximated by
 118 standard finite difference scheme along coordinate directions or auto-differentiation. To circumvent this
 119 obstacle, we use a newly developed discrete divergence operator introduced in [25] to approximate the
 120 divergence operator. Below let us briefly define the discrete divergence operator denoted by $\mathbf{div}_{\tau} \boldsymbol{\tau}$ for any
 121 $\boldsymbol{\tau} \in \Sigma_g = \mathbf{H}_{g,N}^s(\text{div}; \Omega)$, that may be defined for any $\boldsymbol{\tau} \in \Sigma_g = H_{g,N}(\text{div}; \Omega)$ in a similar fashion. The
 122 $\mathbf{div}_{\tau} \boldsymbol{\tau}$ is a piece-wise constant vector field and its restriction on each $K \in \mathcal{T}$ is an approximation to the
 123 average of $\mathbf{div} \boldsymbol{\tau}$, i.e.,

$$\mathbf{div}_{\tau} \boldsymbol{\tau}|_K \approx \text{avg}_K \mathbf{div} \boldsymbol{\tau} = \frac{1}{|K|} \left(\int_{\partial K \setminus \Gamma_N} \boldsymbol{\tau} \mathbf{n} dS + \int_{\partial K \cap \Gamma_N} \mathbf{g}_N dS \right), \quad (16)$$

124 where \mathbf{n} is the outward unit vector normal to ∂K , the boundary of K . Surface integrals in (16) may be
 125 approximated by either proper standard or adaptive numerical integration.

126 Third, the symmetry of $\Sigma_g = \mathbf{H}_{g,N}^s(\text{div}; \Omega)$ for problem (6) can be easily enforced strongly by setting
 127 $\sigma_{ij} = \sigma_{ji}$ so that the stress has only $d_o = 3(d-1)$ variables. The Neumann boundary condition in Σ_g for
 128 both problems becomes an essential boundary condition in the dual formulation (11). One may penalize
 129 the complementary functional in (10) by adding either the $H^{-1/2}$ or a weighted L^2 norm of the residual of
 130 the Neumann boundary condition. This type of treatments has been discussed for the deep Ritz method
 131 (see, e.g., [8]). An attractive feature of the discrete divergence operator defined in (16) is that the Neumann
 132 boundary condition is already weakly enforced. Therefore, it is not necessary to enforce it by adding
 133 penalization terms. Adjusting the penalization coefficient is, in general, nontrivial, and therefore, using the
 134 discrete divergence operator simplifies the training process.

Now, for the simple composite midpoint quadrature rule, we are ready to define the discrete negative complementary functional as

$$J_{\tau}(\boldsymbol{\tau}; \gamma) = \frac{1}{2} a_{\tau}(\boldsymbol{\tau}, \boldsymbol{\tau}; \gamma) - b_{\tau}(\boldsymbol{\tau}; f; \gamma) + \frac{1}{2} c_{\tau}^2(f; \gamma), \quad (17)$$

where $c_{\tau}(f; \gamma) = \sum_{K \in \mathcal{T}} |K| (\gamma f^2)(\mathbf{x}_K)$ for problem (1) and $c_{\tau}(f; \gamma) = \sum_{K \in \mathcal{T}} |K| (\gamma |\mathbf{f}|^2)(\mathbf{x}_K)$ for problem (6), and the discrete quadratic and linear forms are given by

$$a_{\tau}(\boldsymbol{\tau}, \boldsymbol{\tau}; \gamma) = \begin{cases} \sum_{K \in \mathcal{T}} |K| \left\{ \boldsymbol{\tau}^T A^{-1} \boldsymbol{\tau} + \gamma (\text{div}_{\tau} \boldsymbol{\tau})^2 \right\} (\mathbf{x}_K), & \text{problem (1),} \\ \sum_{K \in \mathcal{T}} |K| \left\{ \frac{1}{2\mu} |\boldsymbol{\tau}^D|^2 + \frac{1}{d(2\mu + d\lambda)} |\text{tr} \boldsymbol{\tau}|^2 + \gamma |\mathbf{div}_{\tau} \boldsymbol{\tau}|^2 \right\} (\mathbf{x}_K), & \text{problem (6),} \end{cases}$$

and

$$b_{\tau}(\tau; f, \gamma) = \begin{cases} \sum_{K \in \mathcal{T}} |K| (\gamma f \operatorname{div} \tau)(\mathbf{x}_K) - \sum_{E \in \mathcal{E}_D} |E| (g_D \tau \cdot \mathbf{n})(\mathbf{x}_E), & \text{problem (1),} \\ \sum_{K \in \mathcal{T}} |K| (\gamma \mathbf{f} \cdot \operatorname{div} \tau)(\mathbf{x}_K) + \sum_{E \in \mathcal{E}_D} |E| (\mathbf{g}_D \cdot (\tau \mathbf{n}))(\mathbf{x}_E), & \text{problem (6),} \end{cases}$$

respectively. Then, the dual neural network (DuNN) method is to find $\sigma_{\tau} \in \mathcal{M}_M \cap \Sigma$ such that

$$J_{\tau}(\sigma_{\tau}; \gamma) = \min_{\tau \in \mathcal{M}_M \cap \Sigma} J_{\tau}(\tau; \gamma), \quad (18)$$

135 where $\Sigma = H(\operatorname{div}; \Omega)$ for problem (1) and $\Sigma = \mathbf{H}^s(\operatorname{div}; \Omega)$ for problem (6).

136 To understand the effect of numerical integration and differentiation, we extend the first Strang lemma
137 for the Galerkin approximation over a subspace (see, e.g, [26]) to the DuNN approximation over a subset.

Theorem 1. *Assume that there exists a positive constant α independent of $\mathcal{M}_{2M} \cap \Sigma$ such that*

$$\alpha \|\tau\|_a^2 \leq a_{\tau}(\tau, \tau), \quad \forall \tau \in \mathcal{M}_{2M} \cap \Sigma. \quad (19)$$

Let σ and $\sigma_{\tau} \in \mathcal{M}_M$ be the solutions of (11) and (18), respectively. Then there exists a positive constant C such that

$$\|\sigma - \sigma_{\tau}\|_a \leq C \left(\inf_{\tau \in \mathcal{M}_{2M} \cap \Sigma} \mathbf{E}(\tau) + \sup_{\tau \in \mathcal{M}_{2M} \cap \Sigma} |f(\tau) - f_{\tau}(\tau)| / \|\tau\|_a \right), \quad (20)$$

138 where $\mathbf{E}(\tau) = \|\sigma - \tau\|_a + \sup_{\mathbf{v} \in \mathcal{M}_{2M} \cap \Sigma} |a(\tau, \mathbf{v}) - a_{\tau}(\tau, \mathbf{v})| / \|\mathbf{v}\|_a$.

Proof. For any $\tau \in \mathcal{M}_M \cap \Sigma$, let $\mathbf{e}_{\tau}(\tau) = \sigma^{\epsilon} - \tau$. It is easy to see that

$$J_{\tau}(\sigma_{\tau}^{\epsilon}; \gamma_{\epsilon}) \leq J_{\tau}(\tau; \gamma_{\epsilon}) \quad \text{and} \quad a(\sigma^{\epsilon}, \mathbf{e}_{\tau}(\tau)) = f(\mathbf{e}_{\tau}(\tau)) + g(\mathbf{e}_{\tau}(\tau)),$$

139 where $g(\mathbf{e}_{\tau}(\tau)) =$. This, together with the assumption in (19), implies

$$\begin{aligned} \frac{\alpha}{2} \|\mathbf{e}_{\tau}(\tau)\|_a^2 &\leq \frac{1}{2} a_{\tau}(\mathbf{e}_{\tau}(\tau), \mathbf{e}_{\tau}(\tau)) \leq f_{\tau}(\mathbf{e}_{\tau}(\tau)) - a_{\tau}(\tau, \mathbf{e}_{\tau}(\tau)) \\ &= \left(f_{\tau}(\mathbf{e}_{\tau}(\tau)) - f(\mathbf{e}_{\tau}(\tau)) \right) + \left(a(\tau, \mathbf{e}_{\tau}(\tau)) - a_{\tau}(\tau, \mathbf{e}_{\tau}(\tau)) \right) + a(\sigma - \tau, \mathbf{e}_{\tau}(\tau)). \end{aligned}$$

140 Since $|f(\tau) - f_{\tau}(\tau)| \leq \|\tau\|_a \sup_{\mathbf{w} \in \mathcal{M}_{2M}} |f(\mathbf{w}) - f_{\tau}(\mathbf{w})| / \|\mathbf{w}\|_a$, by the Cauchy-Schwarz inequality and the
141 fact that $\mathbf{e}_{\tau}(\tau) \in \mathcal{M}_{2M}$, we have

$$\|\mathbf{e}_{\tau}(\tau)\|_a^2 \leq C \left(\mathbf{E}(\tau) + \sup_{\tau \in \mathcal{M}_{2M}} |f(\tau) - f_{\tau}(\tau)| / \|\tau\|_a \right).$$

142 Now, the validity of (20) follows from using the triangle inequality and taking infimum over all $\tau \in \mathcal{M}_{2M} \cap \Sigma$.

143 This completes the proof of the theorem. \square

144 Theorem 1 indicates that the total error in the energy norm is bounded by the approximation error of
145 the set of neural network functions plus the numerical integration and differentiation error.

146 *3.3. Constrained minimization*

147 In the case that $\gamma = 0$, i.e., $c = 0$ in (1) or (6), (11) is a constrained minimization problem. One may use
 148 the method of Lagrange multiplier or penalty. The former leads to a saddle point problem and the latter
 149 has difficulty to choose a proper penalization parameter that is good in both accuracy and efficiency. On
 150 one hand, a standard perturbation theory [17] suggests that the penalization parameter (still denoted by γ)
 151 should be $\gamma = \epsilon^{-1}$ with $0 < \epsilon \ll 1$ for accuracy. On the other hand, this choice leads to an ill-conditioned
 152 algebraic problem.

This section introduces an iterative procedure to gradually enforce the equilibrium equation. For simplicity of presentation, we describe the procedure at the continuous level. Let δ_{k-1} be the previous time step size and $u^{(k)}$ and $\mathbf{u}^{(k)}$ are the previous approximation to the solution of problem (1) and problem (6), respectively. Set

$$f^{(k)} = \begin{cases} f + \delta_k^{-1} u^{(k)}, & \text{problem (1),} \\ \mathbf{f} + \delta_k^{-1} \mathbf{u}^{(k)}, & \text{problem (6).} \end{cases}$$

Given the previous approximation $\boldsymbol{\sigma}^{(k)}$ to the solution of (11), define the following negative complementary functional at the k^{th} step by

$$J^{(k)}(\boldsymbol{\tau}) = \frac{1}{2} a(\boldsymbol{\tau}, \boldsymbol{\tau}; \delta_k) - b(\boldsymbol{\tau}; f^{(k)}, \delta_k) + \frac{1}{2} c^2(f^{(k)}; \delta_k). \quad (21)$$

Then the iterative procedure is to find $\boldsymbol{\sigma}^{(k+1)} \in \Sigma_g$ such that

$$J^{(k)}(\boldsymbol{\sigma}^{(k+1)}) = \min_{\boldsymbol{\tau} \in \Sigma_g} J^{(k)}(\boldsymbol{\tau}) \quad (22)$$

and set

$$\begin{cases} u^{(k+1)} = \delta_k (f - \operatorname{div} \boldsymbol{\sigma}^{(k+1)}) + u^{(k)}, & \text{problem (1),} \\ \mathbf{u}^{(k+1)} = \delta_k (\mathbf{f} - \operatorname{div} \boldsymbol{\sigma}^{(k+1)}) + \mathbf{u}^{(k)}, & \text{problem (6)} \end{cases} \quad \text{and } f^{(k+1)} = \begin{cases} f + \delta_k^{-1} u^{(k+1)}, & \text{problem (1),} \\ \mathbf{f} + \delta_k^{-1} \mathbf{u}^{(k+1)}, & \text{problem (6).} \end{cases}$$

153 **4. Numerical Studies**

154 In this section, we present our numerical studies on several second-order elliptic PDEs. Existing NN-based
 155 methods include the deep Ritz [1] and PINN [5], which are based on primal and primitive LS formulations,
 156 respectively. Essential boundary condition(s) (Dirichlet for the primal and both Dirichlet and Neumann
 157 for the primitive LS) are enforced by penalizing them in the loss functional. The deep Ritz has recently
 158 been extended to linear elasticity in [27, 8]. We will compare the proposed DuNN with the aforementioned
 159 NN-based methods.

160 In all experiments, the structure of the DNN used is expressed as $d-n_1-n_2 \cdots n_{l-1}-d_o$ for a l -layer network
 161 with n_1 , n_2 and n_{l-1} neurons in the respective first, second, and $(l-1)$ th layers. The d and d_o represent

162 the input and output dimensions of the network. For DuNN, $d_o = 3(d - 1)$, and for deep Ritz and PINN,
 163 $d_o = d$. The minimization of the loss functionals in all experiments is solved using the Adam optimization
 164 algorithm [28].

165 *4.1. Test Example I: a two-dimensional singularly perturbed reaction-diffusion problem*

Consider the following 2D scalar reaction-diffusion problem:

$$-\varepsilon^2 \Delta u + u = f \quad \text{in } \Omega, \quad u = 0 \quad \text{on } \partial\Omega,$$

166 with the true solution $u = \tanh(\frac{1}{\varepsilon}(x^2 + y^2 - \frac{1}{4})) - \tanh(\frac{3}{4\varepsilon})$ defined in the unit disc $\Omega = \{(x, y) \in \mathbb{R}^2 : x^2 + y^2 < 1\}$. Consider the problem in two cases: $\varepsilon = 0.05$ and $\varepsilon = 0.005$, and note that there is a sharp
 167 interior transition layer at $r = \sqrt{x^2 + y^2} = 1/2$ with a width of order ε in the solution. When ε is small,
 168 there is a numerical difficulty in solving these types of problem.
 169

170 Set the flux $\boldsymbol{\sigma} = -\varepsilon^2 \nabla u$, and with the vanish boundary condition, the corresponding DuNN loss func-
 171 tional using the complementary energy (2) is reduced to

$$J^*(\boldsymbol{\tau}) = \frac{1}{2} \left\{ \|\varepsilon^{-1} \boldsymbol{\tau}\|_{0,\Omega}^2 + \|(\operatorname{div} \boldsymbol{\tau} - f)\|_{0,\Omega}^2 \right\}. \quad (23)$$

172 To compare, we tested the deep Ritz and PINN methods as well. Both deep Ritz and PINN use DNNs
 173 to approximate the primary variable u . Deep Ritz employs the following energy-based loss functional,

$$J(v) = \frac{1}{2} \left\{ \|\varepsilon \nabla v\|_{0,\Omega}^2 + \|v\|_{0,\Omega}^2 + \gamma_D \|v\|_{1/2,\partial\Omega}^2 \right\} - (v, f), \quad (24)$$

174 while PINN uses a direct least square loss functional,

$$L(v) = \|-\varepsilon^2 \Delta v + v - f\|_{0,\Omega}^2 + \gamma_D \|v\|_{0,\partial\Omega}^2, \quad (25)$$

175 where γ_D is the penalization coefficient.

176 Table 1 reports the results of the three methods. As shown in the table, for both material cases and
 177 the three different DNN structures (a three-layer DNN with 128 neurons in the hidden layer, and two four-
 178 layer DNNs with 64 and 96 neurons in the hidden layer, respectively), DuNN achieves better accuracy in
 179 approximating the flux $\boldsymbol{\sigma}$, and Deep Ritz performs better in approximating the primary variable u . As
 180 illustrated in Figure 2, the DuNN method yields a direct approximation of the flux $\boldsymbol{\sigma}$, which results in fewer
 181 numerical oscillations; see Figures 2(a) and 2(b). The other two methods calculate the flux $\boldsymbol{\sigma}$ indirectly
 182 using $\boldsymbol{\sigma} = -\varepsilon^2 \nabla u$, which involves a differential operation ³ on the DNN output function u . As shown in
 183 Figures 2(d) 2(e) and 2(g) 2(h)), this leads to some numerical oscillations in flux simulation.

³In our experiments, numerical differentiation was used to obtain the results

Table 1: Relative L^2 errors for test example I using three DNN structures (2-128-128- d_o | 2-64-64-64- d_o | 2-96-96-96- d_o , where $d_o = 2$ for DuNN, and $d_o = 1$ for PINN and Deep Ritz).

	Method	$\frac{\ u - u^N\ }{\ u\ }$	$\frac{\ \sigma - \sigma^N\ }{\ \sigma\ }$
$\varepsilon = 0.05$	PINN	13.19% 12.63% 12.38%	48.04% 42.63% 37.97%
	Deep Ritz	0.984% 0.910% 0.904%	16.73% 12.00% 12.07%
	DuNN	4.248% 2.682% 2.227%	4.957% 2.826% 2.190%
$\varepsilon = 0.005$	PINN	8.522% 5.814% 2.727 %	73.01% 57.81% 34.33%
	Deep Ritz	2.382% 1.056% 0.997%	32.18% 28.67% 28.49%
	DuNN	3.019% 1.751% 1.524%	24.04% 12.57% 9.385%

***training details:**

1. Activation function: ReLU;
2. numerical integration: 400×360 uniformly distributed quadrature points;
3. Adam optimization: 80,000 iterations; learning rate starts with 0.004 and decays 50% per 10,000 iterations;
4. penalization coefficient in loss function: for PINN, $\gamma_D = 100$, and for Deep Ritz, $\gamma_D = 1$.

184 *4.2. Test Example II: two-dimensional Poisson Equation*

The second test problem is a two-dimensional Poisson equation defined on a square unit $\Omega = (0, 1) \times (0, 1)$. The exact solution for the primary variable $u = \sin(\frac{\pi}{2}x)\sin(\pi y) + x^2y^2$. And the dual variable σ has the analytic form,

$$\sigma = -\nabla u = \begin{pmatrix} -\frac{\pi}{2}\cos(\frac{\pi}{2}x)\sin(\pi y) - 2xy^2 \\ -\pi\sin(\frac{\pi}{2}x)\cos(\pi y) - 2x^2y \end{pmatrix}.$$

185 With the right-hand side $f = \text{div } \sigma = \frac{5\pi^2}{4}\sin(\frac{\pi}{2}x)\sin(\pi y) - 2(x^2 + y^2)$, and the Dirichlet boundary condition
186 defined in $x = 0$ and $y = 0$, the Neumann boundary prescribed in $x = 1$ and $y = 1$, we tested the
187 performance of DuNN and compared it with the deep Ritz and PINN. Specifically, for DuNN, since the
188 primary variable term vanishes in the Poisson equation ($c = 0$), we tested two approaches to solve the
189 corresponding constrained minimization problem. The first is the penalization method that uses the added
190 penalty term $\gamma \|(\text{div } \tau - f)\|_{0,\Omega}^2$, where γ is a penalization coefficient that needs to be adjusted. And the
191 second method is the outer-inner iterative procedure using pseudo-time described in section 3.3.

192 Using the penalization method, DuNN needs to tune one parameter γ for the force balance term, deep
193 Ritz needs one parameter γ_D for the Dirichlet boundary condition term, and PINN needs two parameters,
194 γ_D and γ_N for both the Dirichlet and Neumann boundary condition terms. Table 2 reports the results of the
195 comparison. In all three methods, we adjusted the penalization coefficients in their respective loss functions
196 and reported the best results. Note that in the DuNN method, the primary variable u is reconstructed
197 using another DNN of the same structure (2-50-50-1), and the loss function for reconstructing u is $L(v) =$

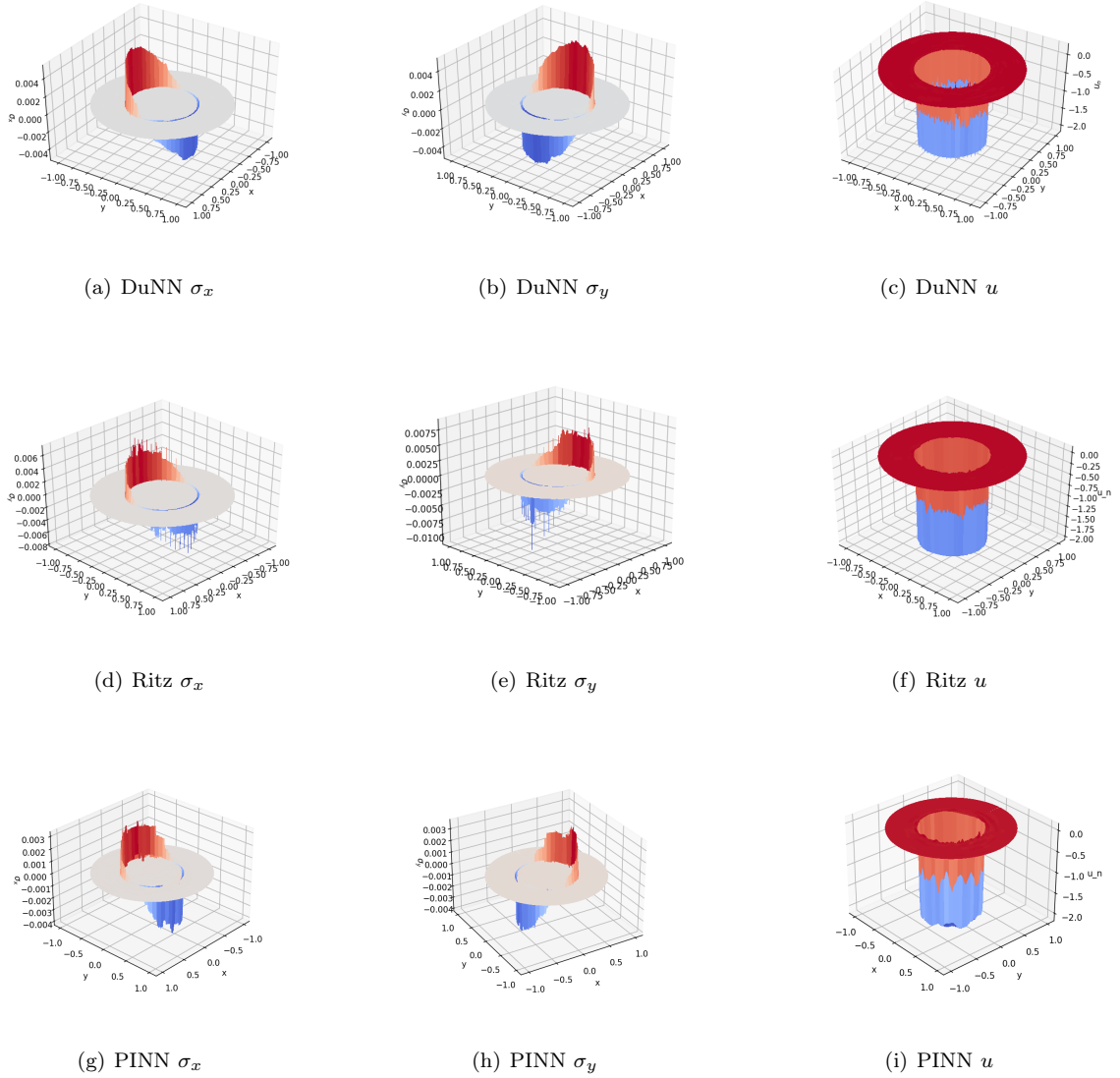


Figure 2: Numerical Results of test example I ($\varepsilon = 0.005$) using three NN-based methods.

198 $\|\nabla v + \sigma_N\|_{0,\Omega}^2 + \gamma_D \|v - g_D\|_{0,\partial\Omega}^2$, where σ_N is the obtained numerical flux from DuNN. The tuned penalization
 199 parameters are shown in the second row of the table 2. From the error measures shown in the last row of
 200 the table, we can see that for smooth problems like the one in this test, all three methods perform well if
 201 the hyper parameters are tuned into the appropriate scales.

202 We then tested the outer-inner pseudo-time method for the constrained minimization problem. The
 203 same DNN structure (2-50-50-2) and activation function (Sigmoid) were used as in the penalization method
 204 previously. In the experiment, the pseudo-time step size remained constant throughout the outer-inner
 205 iterations. Table. 3 records the numerical results of using different pseudo-time step sizes δ . It is found that

Table 2: Relative L^2 errors for test example II using penalization method (DNN structure: 2-50-50- d_o).

DuNN		Deep Ritz		PINN	
$\gamma = 20$		$\gamma_D = 1000$		$\gamma_D = 10000, \gamma_N = 10000$	
$\frac{\ \mathbf{u} - \mathbf{u}^N\ }{\ \mathbf{u}\ }$	$\frac{\ \boldsymbol{\sigma} - \boldsymbol{\sigma}^N\ }{\ \boldsymbol{\sigma}\ }$	$\frac{\ \mathbf{u} - \mathbf{u}^N\ }{\ \mathbf{u}\ }$	$\frac{\ \boldsymbol{\sigma} - \boldsymbol{\sigma}^N\ }{\ \boldsymbol{\sigma}\ }$	$\frac{\ \mathbf{u} - \mathbf{u}^N\ }{\ \mathbf{u}\ }$	$\frac{\ \boldsymbol{\sigma} - \boldsymbol{\sigma}^N\ }{\ \boldsymbol{\sigma}\ }$
0.740%	1.307%	0.949%	3.730%	0.594%	1.3224%

***training details:**

1. activation function: Sigmoid;
 2. numerical integration: 100×100 uniform distributed quadrature points ($h = 0.02$).
 3. Adam optimization: 200,000 iterations;
- learning rate starts with 0.01 and decays 90% per 20,000 iterations until reaches $1e-5$.

Table 3: Relative L^2 errors for test example II using pseudo-time method (DNN structure: 2-50-50-2).

Time step size δ	0.1	0.05	0.01	0.005	0.001
Inner iteration per time step	5,000	2,500	500	250	50
Outer iteration number	20	40	200	400	2000
$\frac{\ \boldsymbol{\sigma} - \boldsymbol{\sigma}^N\ }{\ \boldsymbol{\sigma}\ }$	0.273%	0.221%	0.182%	0.134%	0.173%

***training details:**

1. Total number of iterations: 100,000;
2. learning rate is $1e-3$ for the first 50,000 iterations and $1e-4$ for the rest.

206 the pseudo-time iterative method, compared to the penalization method, is less sensitive to the parameter
 207 (time-step size) and converges to a better solution in fewer iterations (a total of 100,000 iterations). We also
 208 observed that, in general, a larger step size requires more inner iterative steps, as reported in the second
 209 row of the table. Figure. 3(a) and 3(b) plot the numerical results for the approximate flux σ using the time
 step size $\delta = 0.005$.

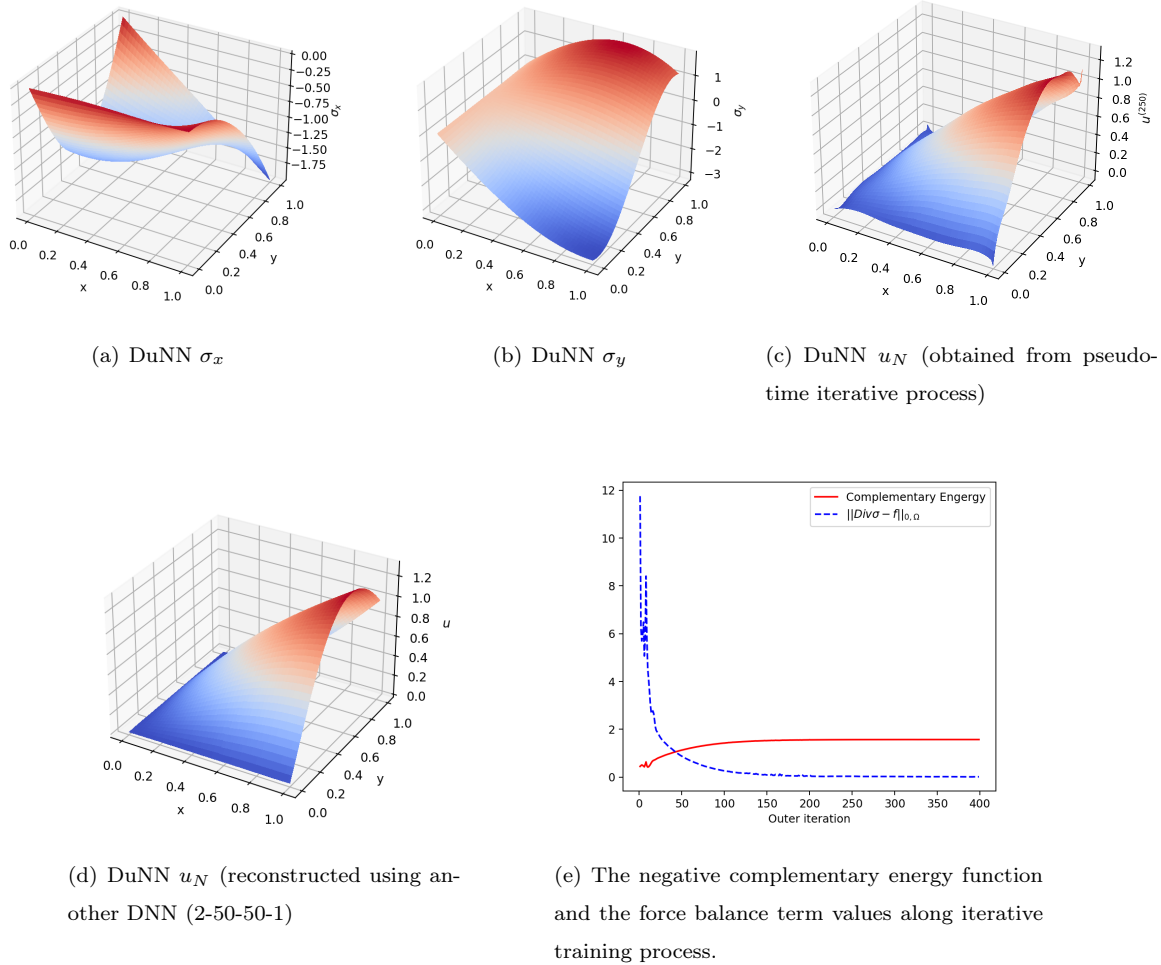


Figure 3: Numerical Results of Poisson equation using pseudo-time outer-inner iterative method ($\delta = 0.005$).

210
 211 Another benefit of the pseudo-time method is that the added term u_t converges to u_N , becoming a
 212 byproduct of the iterative process. Figure 3(c) illustrates the resulting u_N . Alternatively, one may also
 213 reconstruct u_N using another DNN, as previously used. Recovering u_N using another DNN requires addi-
 214 tional time and resources to form the approximated primary variable u , but produces a smoother result in
 215 this case, as shown in Figure 3(d). The effectiveness of the pseudo-time method is further demonstrated in
 216 Figure 3(e). For each time step, the force balance term $\|(\operatorname{div} \tau - f)\|_{0, \Omega}^2$ continuously decays to nearly zero,

217 and the negative complementary energy converges to the true value of this problem, which is 1.571.

218 *4.3. Test Example III: L-shaped linear elastic plate under stress*

The last test example is a common benchmark problem for linear elasticity equation (6) featuring a re-entrant corner and a resulting point singularity[29]. This problem is posed on a L -shaped domain $\Omega = (-1, 1)^2 \setminus ([0, 1] \times [-1, 0])$ with a body force $\mathbf{f} = \mathbf{0}$. The analytical solution for displacement \mathbf{u} is,

$$\mathbf{u} = [A \cos \theta - B \sin \theta, A \sin \theta - B \cos \theta]^T,$$

where A and B are defined in polar coordinates:

$$\begin{cases} A = \frac{r^\alpha}{2\mu} \left(-(1 + \alpha) \cos((1 + \alpha)\theta) + C_1(C_2 - 1 - \alpha) \cos((1 - \alpha)\theta) \right), \\ B = \frac{r^\alpha}{2\mu} \left((1 + \alpha) \sin((1 + \alpha)\theta) - C_1(C_2 - 1 + \alpha) \sin((1 - \alpha)\theta) \right). \end{cases}$$

219 Here $\alpha \approx 0.544483737$ is the *critical* exponent and the definition of C_1, C_2 together with the exact form of
 220 stress $\boldsymbol{\sigma}$ are referenced in [29]. We tested two materials with Young's modulus $E = 100000$ and Poisson's
 221 ratio $\nu = 0.3$ for a compressible material and $\nu = 0.49999$ for a nearly incompressible material. The Lamé
 222 constants are given by $\mu = \frac{E}{2(1+\nu)}$ and $\lambda = \frac{E\nu}{(1+\nu)(1-2\nu)}$.

223 The method of PINN does not apply here due to the existence of a stress singularity at the origin point
 224 $(0, 0)$. Therefore, we compare only the numerical results of the two energy-based methods: Deep Ritz [8]
 225 and DuNN.

226 **Material case I** ($\nu = 0.3$): we used only the penalization method in this case. For penalization
 227 coefficients, we tested various values and finally adjusted them to $\gamma = 1e - 4$ for DuNN and $\gamma_D = 10$ for
 228 deep Ritz. Uniform quadrature methods with the midpoint quadrature rule and two set of the integration
 229 mesh sizes were tested and the corresponding results are reported in Table 4. The numerical experiments
 230 show that both energy-based methods (deep Ritz and DuNN) have the capability of handling reentrant corner
 231 singularity, while DuNN performs better in terms of relative L^2 approximation error for the numerical stress,
 232 using both integration mesh sizes.

233 **Material case II** ($\nu = 0.49999$): since the deep Ritz method does not accurately characterize the
 234 stress under the near-incompressible condition (locking phenomenon), we tested DuNN alone and compared
 235 the penalization method with the pseudo-time method for the constrained minimization problem. Both
 236 the uniform and non-uniform quadrature methods were tested in this material case. For the non-uniform
 237 quadrature method, a manual integration mesh was constructed using progressive refinement near the singu-
 238 lar point (see the corresponding non-uniform quadrature points in Figure 3(d)). Note that this non-uniform
 239 integration mesh can be constructed adaptively using the adaptive quadrature refinement (AQR) method
 240 proposed in [8]. Since numerical integration is not a main focus of this work, we used this manually generated
 241 set of quadrature points to investigate the effect of numerical integration.

242 From the result shown in Table 4, we can see that both the penalization method and the pseudo-time
 243 method can handle incompressibility and simulate the stress distribution with point singularity reasonably
 244 well. The non-uniform quadrature method produced slightly better result with fewer number of quadrature
 245 points. During the training process, we also observed that the pseudo-time-based minimization, although
 246 also having a time step δ_t parameter to be determined, converges faster due to the gradual enforcement
 247 of the equilibrium equation. In this test, the penalization method required 200,000 iterations, while the
 248 pseudo-time method required less than 10,000 iterations to converge. The corresponding numerical results
 249 are plotted in Figure 4, where subfigures (a)-(c) represent the numerical stress distributions of DuNN.
 250 The results show that both the point singularity and incompressibility of the material are well handled
 251 using DuNN. Figure 4(e) illustrates the pseudo-time-based negative complementary function minimization
 252 process. During the iterative process, the force balance term quickly decreases to near zero, while the
 253 negative complementary energy converges to its theoretic value.

Table 4: Relative L^2 errors of numerical stress for the L -shaped problem(Network: 2-48-48-48- d_o , Activation: sigmoid)

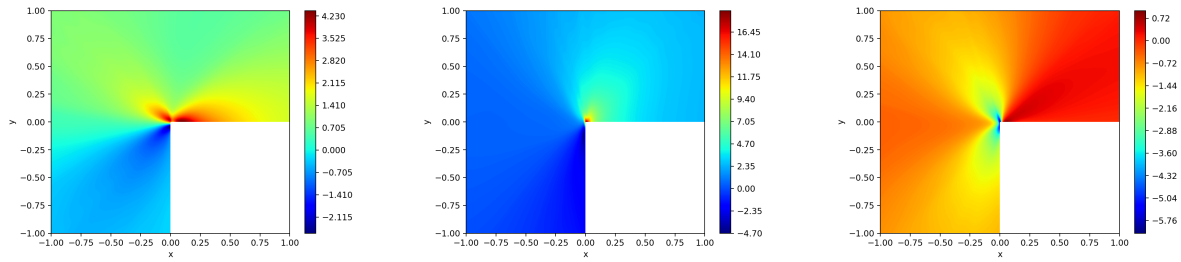
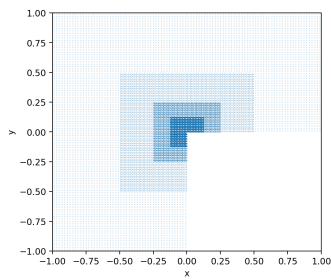
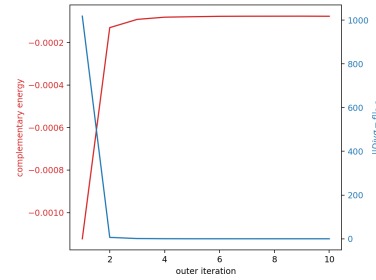
	Method	Quadrature	$\frac{\ \sigma - \sigma_N\ }{\ \sigma\ }$
$\nu = 0.3$	Deep Ritz (penalization)	uniform $h = 0.02$	38.59 %
		uniform $h = 0.01$	31.62 %
	DuNN (penalization)	uniform $h = 0.02$	10.81 %
		uniform $h = 0.01$	10.08 %
$\nu = 0.49999$	DuNN (penalization)	uniform: $h = 0.01$	12.44 %
		Non-uniform	12.39 %
	DuNN (pseudo-time)	uniform $h = 0.01$	10.96%
		Non-uniform	10.30%

***training details:**

1. penalization Method: DuNN: $\gamma = 1e - 4$, Deep Ritz: $\gamma_D = 10$
 200,000 iterations and learning rate starts from 0.01 and decays 50% every 50,000 iterations.
2. pseudo-time method: $\delta = 1e - 6$
 inner iteration: 10,000; number of time-step:10; total iteration: 100,000 .

254 5. Conclusion

255 In this paper, we established a physics-driven deep neural network-based computational framework to
 256 solve elliptic partial differential equations and systems. The problem is formulated as an optimization of
 257 the complementary energy functional with the benefit of using the sole dual variable. Combined with the

(a) σ_{xx} (b) σ_{yy} (c) σ_{xy} (d) 30465 non-uniform quadrature points (from $h = 1/50$, refined 3 times to 24,543 points)

(e) The complementary energy and the force balance term along training process

Figure 4: Numerical results using DuNN for the L -shaped elastic plate problem, case II ($\nu = 0.49999$) (structure: 2-48-48-48-3, activate function: sigmoid, non-uniform quadrature and pseudo-time outer-inner iterative method).

258 physics-preserved discrete divergence operator, all boundary conditions can be enforced naturally without
 259 using any penalization term. For problems without the primary variable term, a pseudo- time-based iterative
 260 method was developed to gradually enforce the equilibrium equation.

261 Numerical studies demonstrate that DuNN accurately approximates dual variables for elliptic problems.
 262 Compared to existing neural network-based methods, DuNN offers superior flux prediction accuracy and is
 263 applicable to a broader range of problems, including those with discontinuities or singularities. It is also
 264 effective for problems involving both compressible and incompressible materials.

265 Acknowledgments

266 This work was supported in part by the National Science Foundation under grant DMS-2110571 and we
 267 thank the support of DARPA project on symbiotic design and Stanford Research International (SRI) for
 268 partial support of the project.

269 **References**

- 270 [1] W. E. B. Yu, The deep Ritz method: A deep learning-based numerical algorithm for solving variational problems, *Com-*
271 *munications in Mathematics and Statistics* 6 (1) (2018) 1–12.
- 272 [2] J. Berg, K. Nystrom, A unified deep artificial neural network approach to partial differential equations in complex geome-
273 *tries*, *Neurocomputing* 317 (2018) 28–41.
- 274 [3] J. Sirignano, K. Spiliopoulos, DGM: A deep learning algorithm for solving partial differential equations, *Journal of Com-*
275 *putational Physics* 375 (2018) 1139–1364.
- 276 [4] M. Raissi, G. E. Karniadakis, Deep hidden physics models: Deep learning of nonlinear partial differential equations, *J.*
277 *Mach. Learning Res.* 19 (1) (2018) 932–955.
- 278 [5] M. Raissi, P. Perdikaris, G. E. Karniadakis, Physics-informed neural networks: A deep learning framework for solving
279 *forward and inverse problems involving nonlinear partial differential equations*, *Journal of Computational Physics* 378
280 (2019) 686–707.
- 281 [6] Y. Bar-Sinai, S. Hoyer, J. Hickey, M. P. Brenner, Learning data-driven discretizations for partial differential equations,
282 *Proceedings of the National Academy of Science of USA* 116 (31) (2019) 15344–15349.
- 283 [7] Z. Cai, J. Chen, M. Liu, X. Liu, Deep least-squares methods: An unsupervised learning-based numerical method for
284 *solving elliptic PDEs*, *Journal of Computational Physics* 420 (2020) 109707.
- 285 [8] M. Liu, Z. Cai, K. Ramani, Deep Ritz method with adaptive quadrature for linear elasticity, *Computer Methods in Applied*
286 *Mechanics and Engineering* 415 (2023) 116229.
- 287 [9] I. Daubechies, R. DeVore, S. Foucart, B. Hanin, G. Petrova, Nonlinear approximation and (deep) ReLU networks, arXiv
288 *preprint arXiv:* (2019).
- 289 [10] R. DeVore, B. Hanin, G. Petrova, Neural network approximation, *Acta Numerica* 30 (2021) 327–444. doi:10.1017/
290 *S0962492921000052*.
- 291 [11] D. Yarotsky, Error bounds for approximations with deep ReLU networks, *Neural Networks* 94 (2017) 103–114.
- 292 [12] J. Xu, The finite neuron method and convergence analysis, *Communications in Computational Physics* 28 (2020) 1707–
293 1745.
- 294 [13] M. Liu, Z. Cai, Adaptive two-layer ReLU neural network: II. Ritz approximation to elliptic PDEs, *Computers. Math.*
295 *Appl.* 113 (2022) 103–116.
- 296 [14] Z. Cai, J. Chen, M. Liu, Least-squares ReLU neural network (LSNN) method for linear advection-reaction equation,
297 *Journal of Computational Physics* 443 (2021) 110514.
- 298 [15] I. Ekeland, R. Témam, *Convex Analysis and Variational Problems*, Society for Industrial and Mathematics, Philadelphia,
299 1999.
- 300 [16] S. Zhang, Primal-dual reduced basis methods for convex minimization variational problems: robust true solution a poste-
301 *riori error certification and adaptive greedy algorithms*, *SIAM J. Sci. Comput.* 42 (1) (2020) A3638–A3676.
- 302 [17] F. Brezzi, M. Fortin, *Mixed and Hybrid Finite Element Methods*, Springer-Verlag, New York, 1991.
- 303 [18] Z. Cai, G. Starke, Least-squares methods for linear elasticity, *SIAM J. Numer. Anal* 42 (2) (2004) 826–842.
- 304 [19] Z. Cai, B. Lee, P. Wang, Least-squares methods for incompressible newtonian fluid flow: linear stationary problems, *SIAM*
305 *J. Numer. Anal* 42 (2) (2004) 843–859.
- 306 [20] A. Pinkus, Approximation theory of the MLP model in nueral networks, *Acta Numerica* 15 (1999) 143–195.
- 307 [21] G. Cybenko, Approximation by superpositions of a sigmoidal function, *Mathematics of Control, Signals, and Systems* 2
308 (1989) 303–314.
- 309 [22] K. Hornik, M. Stinchcombe, H. White, Multilayer feedforward networks are universal approximators, *Neural Networks* 2
310 (1989) 359–366.
- 311 [23] L. Schumaker, *Spline Functions: Basic Theory*, John Wiley, New York, 1981.

- 312 [24] M. Liu, Z. Cai, J. Chen, Adaptive two-layer ReLU neural network: I. best least-squares approximation, *Computers. Math.*
313 *Appl.* 113 (2022) 34–44.
- 314 [25] Z. Cai, J. Chen, M. Liu, Least-squares ReLU neural network (LSNN) method for scalar nonlinear hyperbolic conservation
315 laws: discrete divergence operator, *J. Comput. Appl. Math.* 433 (2023) 115298.
- 316 [26] P. G. Ciarlet, *The finite element method for elliptic problems*, Society for Industrial and Applied Mathematics, 1978.
- 317 [27] W. Li, M. Z. Bazant, J. Zhu, A physics-guided neural network framework for elastic plates: Comparison of governing
318 equations-based and energy-based approaches, *Computer Methods in Applied Mechanics and Engineering* 383 (2021)
319 113933.
- 320 [28] D. P. Kingma, J. Ba, Adam: A method for stochastic optimization, in: *International Conference on Representation*
321 *Learning*, San Diego, 2015.
- 322 [29] G. Harper, J. Liu, S. Tavener, B. Zheng, Lowest-order weak Galerkin finite element methods for linear elasticity on
323 rectangular and brick meshes, *J. Sci. Comput.* 78 (3) (2019) 1917–1941.